Acta Physica Universitatis Comenianae
Vol. L–LI, Number 1&2 (2009–2010) 95–104

Probe Measurements on a Cavity-Hollow Cathode Discharge Used as Sputter Source for Titanium*

R. Schrittwieser[1], A. Murawski[1], I. Vojvodic[2], C. Ionita[1], S. B. Olenici[3], S. Jaksch[1], P. Scheier[1]

[1]Institute for Ion Physics and Applied Physics, University of Innsbruck, Austria
[2]Faculty of Natural Sciences and Mathematics, University of Montenegro, Podgorica, Montenegro
[3]Faculty of Physics, Alexandru-Ioan-Cuza University of Iasi, Iasi, Romania

Abstract: A cavity-hollow cathode was investigated for its properties as plasma source, versatile low-cost sputtering source and cluster source. The discharge is produced in argon gas inside a hollow cathode consisting of two specifically formed disks of the material to be sputtered. An additional cavity further increases the electron density by the pendulum effect and thereby the production of positive argon ions and the sputter rate. Here we present investigations of this discharge by Langmuir probes. Evidence was found for the formation of a space charge double layer above the cathode. Immediately after their production the sputtered atoms appear to form clusters which are negatively charged. This enhances the deposition rate of the clusters on the substrates. For various sputter durations films of titanium were produced on highly oriented pyrolytic graphite (HOPG). In this case an approximate value for the size of deposited Ti-clusters could be found in investigations by means of a scanning tunnel miscroscope.

Keywords: Cavity hollow cathode, cluster formation, sputtering, Langmuir probe, titanium films.

1. Introduction

Various techniques are in use for thin film depositions. Magnetron sputtering sources are regularly used with great success. However, there are problems with the deposition of ferromagnetic materials. Therefore also alternative sputtering configurations without magnetic fields are investigated. These can also be used for the production of metal ions and as cluster sources [1–3]. Such an alternative is offered by the hollow cathode. Its main advantage is that, on the inner side of the annular cathode cylinder, ion-rich sheaths form due to the cathode fall of the discharge. For the electrons, this leads to the formation of a potential trough a few hundred volts height inside which they can perform a pendulum motion. This effect, which strongly enhances the electron density and thus the ionization rate, gives rise to a high plasma density. This effect is known for a long time, see e.g. [4] and more recently [5, 6]. Often an additional cavity further enhances this effect wherefore this is called the **c**avity **h**ollow **c**athode (CHC). In this case a plasma jet is formed at the muzzle of the hollow cathode. The anode can either be the chamber wall or a special anode ring in a distance of a few cm above the muzzle of the hollow cathode.

As a sputtering source the CHC was first described in [7, 8]. In this case the cathode is made of the material to be sputtered. The plasma ions inside the CHC are accelerated by

*) *Dedicated to Professor Peter Lukáč on the occasion of his 70th birthday.*

the cathode fall towards the inner cathode walls, which causes intensive sputtering. Due to pressure and electric potential gradients the sputtered atoms are transported towards the substrate usually positioned near the anode.

The CHC operates in the range of a few 0.1 mbar and it was used to grow TiN_xO_y-thin films. Good quality thin films of TiN, Ni and Fe were successfully produced by various groups [9 11]. Recently this configuration was intensively investigated, both in the dc regime as well as in the pulsed regime [11, 12].

Since it does not need a magnetic field, one of the main advantages of the CHC configuration is offered by the possibility to sputter also ferromagnetic materials [13]. Moreover, the film quality is enhanced by intense bombardment of the substrate by electrons. It was also shown that during the deposition clusters were formed [14] which are negatively charged in the plasma. To improve the performances of this configuration regarding the control of film parameters (vapour fluency, growth rate, film uniformity, energy of ions impinging on the substrate, size of the sputtered aggregates, elemental composition), further characterization of the CHC is necessary. Here, we concentrate on the presentation and discussion of the results of probe measurements in the CHC plasma and the sputtering of titanium thin films on **h**ighly **o**riented **p**yrolytic **g**raphite (HOPG). The thin films were investigated by a **s**canning **t**unneling **m**icroscope (STM).

2. Experimental set-up and typical discharge data

In general any hollow cathode geometry needs to satisfy the following conditions in order to establish the hollow cathode (HC-) effect[15, 16]:

- The surfaces of the cathode have to face each other, or preferably are formed by an annular cylinder,
- The surfaces have to be separated from each other by a distance such that the high energy electrons generated in one cathode fall can reach the opposite cathode fall without too many collisions, being reflected there.

Obviously the latter condition depends mainly on the plasma density, since, on one side, the mean free path is determined by it, and on the other side, the typical thickness d of an ion rich sheath is determined by the Child-Langmuir's law and thus d^2 is proportional to $V_c^{3/2} / I_i$ with V_c being the voltage across the cathode fall and I_i is the ion current through it, which itself is mainly determined by the plasma density. The inverse of this ratio, i.e., $I_i / V_c^{3/2}$, is, by the way, the perveance of the system.

A schematic presentation of the hollow cathode used in our experiments is shown in Fig. 1. Fig. 2 shows a photo of the CHC, broken down into the main parts. The hollow cathode consists of two specifically shaped disks of the material to be sputtered, with 18.3 mm in diameter, manufactured of the material to be sputtered. The lower disk has a height of 9 mm, the upper one of 7 mm. The upper disk has a conically widening muzzle, opening upwards. The two disks are separated by a glass spacer, 15 mm in diameter and a height between 6-7 mm. The disks and the glass spacer confine a 1.25 cm^3 cylindrical cathode chamber, visible through the glass spacer for optical measurements [11, 12]. The additional cylindrical cavity (5 mm diameter) inside the lower disk further enhances the ionization rate in the hollow cathode [7].

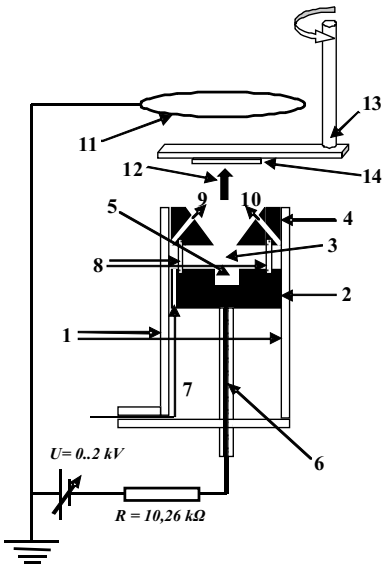

Fig. 1. Schematic of the Cavity Hollow Cathode sputtering source with electronic circuit: 1 glass tube, 2, 4 Ti-disks, 3 cathode chamber, 5 cathode cavity, 6 lead for biasing cathode, 7, 9, 10 gas channels for admission of working gas in front of cathode, 8 glass ring spacer, 11 Cu-ring anode of 3 cm diameter about 5 cm above cathode, 12 plasma jet, 13 pivoting substrate holder, 14 highly oriented pyrolytic graphite (HOPG) substrate. Instead of the pivoting holder sometimes a Langmuir probe was inserted for electric diagnosis of the plasma jet.

Fig. 2. Photo of the CHC, broken down into the main parts.

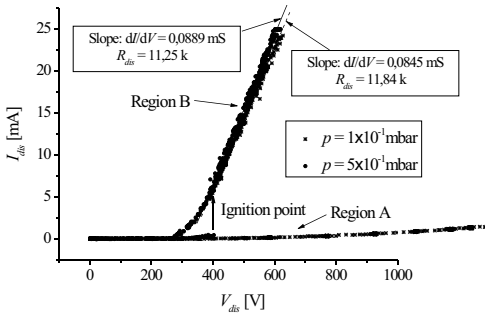

Fig. 3. Current-voltage characteristic of the CHC for two different pressures as indicated in the figure: Region A indicates the glow discharge regime, Region B the hollow cathode regime.

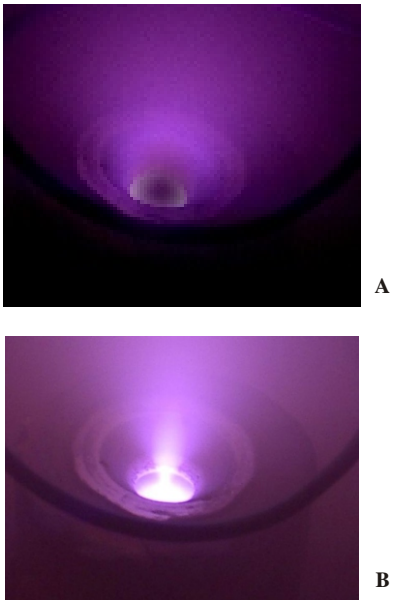

Fig. 4. Photos of the discharge in the CHC muzzle: as in Fig. 3, **A** indicates the glow discharge regime, **B** the hollow cathode regime.

However, after about 1 / 2 hour operation the glass spacer becomes coated on the inside by the cathode material. This not only restricts the time for optical investigations but also creates an electrical contact between the lower and upper part of the cathode. Therefore eventually both parts are on the same negative voltage.

The cathode ensemble is introduced into a cylindrical glass tube. The grounded wall of the 5 l stainless steel discharge chamber (not shown in Figs. 1 and 2) acts as the anode. In certain experiments, an additional 30 mm diameter ring anode, situated 5 cm above the upper cathode disk, was used. The substrate is pivoted into the space above the muzzle by a special holder whose distance from the muzzle can be varied up to a few cm. This reduces the deposition rate of titanium on the substrate as long as it is outside. To completely prevent unwanted deposition, a shutter can be inserted additionally into the plasma jet. Instead of the pivoting holder, Langmuir probes were inserted for electrical diagnosis of the plasma jet.

After evacuation to a base pressure of 10^{-5} mbar, Ar gas is employed in front of the upper cathode disk through three inlets (see Fig. 1) up to the working pressure of 0.2 mbar. Typical current-voltage (I_{dis}-V_{dis}) characteristics of the CHC for two different pressures, namely 1 10^{-1} mbar and 5 10^{-1} mbar, are shown in Fig. 3; here I_{dis} is the total current through the system, and V_{dis} is the voltage applied to the CHC. Fig. 4 shows photos into the upper CHC disk muzzle. At low currents, a "pre-discharge" is observed (Region A in Fig. 3 and photo **A** in Fig. 4), classified as a glow discharge created only outside the cathode structure between the upper disk of the CHC and the anode. As the current increases, for a certain ignition voltage the system suddenly jumps into the HC-discharge mode. This operating regime of the discharge (Region B in Fig. 3 and photo **B** in Fig. 4) is characterized by a dramatic increase of I_{dis}. When this occurs, the negative glow is confined inside the cavity, and a conical glowing plasma jet exits from the cathode muzzle, its shape being determined by electrical and pressure gradients. At a pressure of 1 10^{-1} mbar the ignition voltage is close to 1 300 V, decreasing with increasing pressure to around 400 V for 5 10^{-1} mbar. The (I_{dis}-V_{dis}) characteristic shows linear behaviour with its inverse slope representing the resistance of the discharge R_{dis}.

Before the substrate was pivoted into the plasma jet, or the shutter opened, respectively, a few minutes waiting time was necessary since the discharge needed some time to attain constant conditions. Without shutter, even though the substrate was not situated inside the plasma jet, sometimes there was already a certain coating during this waiting time.

The titanium thin films were investigated by means of an STM after taking them out from the CHC and inserting them into the STM. Since the films were exposed to air during this procedure, the Ti-layers became oxidized. For future investigations the CHC will be built into another vacuum connected to the STM chamber by a large valve. Thereby, after thin film deposition, the substrate can directly be transferred into the STM and investigated without being exposed to the air.

3. Experimental results

In several earlier works the formation of an electron beam was postulated appearing above the muzzle of the CHC [9, 11, 17]. Such an electron beam could only be created by a

plasma double layer (DL) [18]. DLs often appear in plasmas with strong electron currents especially at sudden variations of the diameter of the current channel since there the current density changes. This is well known since the times of Langmuir [19]. Thus it seems plausible that also the widening of the channel of the CHC in the upper disk could give rise to the formation of a DL. To substantiate this assumption we have carried out an extensive investigation with Langmuir probes (see Section 3.1. below). See also [20]. In the electric field of a DL, also other negative charge carriers can be accelerated towards the substrate, in addition to the effect of the pressure gradient in this region. As we will see below, there is evidence for the formation of Ti-clusters in the plasma jet, which usually become negatively charged and can thus be accelerated by the DL towards the substrate. This would explain our findings in context with the Ti-clusters, as discussed in Section 3.2.

3.1. Characterisation of the hollow cathode regime by a Langmuir probe

Electrostatic probe measurements were performed with a single Langmuir probe above the CHC muzzle. See Fig. 5 for a schematic of the probe. The probe tips have to be of a refractory metal to avoid excessive sputtering or melting. Therefore, a tungsten wire with a diameter of 0.125 mm was used. The tip is protruding by 1 mm from the probe shaft, a ceramic tube (Al_2O_3) of 0.5 mm in diameter with a borehole of 0.2 mm diameter. Inside the tube the W-wire is spliced on a length of about 20 mm with a certain number of very fine copper wires (threads). This method not only provides an excellent electrical contact but also a good mechanical one between the two different metals due to the softness of the Cu-threads on one side and the roughness of the surface of the W-wire on the other side [21, 22]. This effect is enhanced when the number of Cu-threads is assessed so that the spliced W-Cu-wire fits tightly into the borehole. The ceramic tube is used to insulate the probe wire from the plasma except for a short length (1 mm) and to avoid perturbation of the plasma by the probe shaft. To avoid excessive perturbation of the plasma by the probe, the diameter of the ceramic tube should be as small as possible. Care has also to be taken that there is no electrical contact with any conducting coating that may deposit on the insulator. Eventually the 0.5 mm ceramic tube is fixed by a ceramic glue on top of a 1.2 mm ceramic tube with 4 holes. The probe wire (spliced Cu-threads) is pulled through one of the holes and connected by soldering to a further electrical lead and the vacuum feed-through.

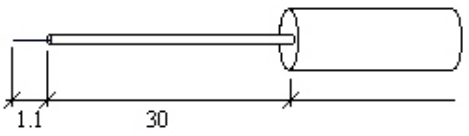

Fig. 5. Schematic of the straight Langmuir probe used for measurements above the CHC muzzle. The probe tip is of tungsten wire with a diameter of 0.125 mm. Inside the ceramic tube of 0.5 mm, outer diameter with a borehole of 0.2 mm diameter, the wire is spliced with a number of very fine copper wires.

The operating pressures were between 1 10^{-1} and 5 10^{-1} mbar. The discharge current was varied and different horizontal and vertical probe positions above the cathode muzzle were applied. The Langmuir probe was electrically swept from –70 V up to +70 V. In order to analyse the current-voltage (I_p-V_p) characteristics of the Langmuir probe, the cylindrical probe theory was applied to determine the plasma parameters such as floating potential V_{fl}, plasma potential $_{pl}$, electron temperature T_e and electron density n_e [23].

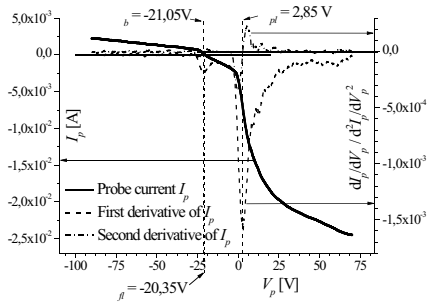

Fig. 6. I_p-V_p characteristic (solid line and symbols) with its first (dashed line) and second (dashed-dotted line) derivative of a single Langmuir probe for I_{dis} = 20 mA, at a pressure p = 1 10^{-1} mbar, registered 10 mm above the cathode and 0 mm horizontal displacement. Please take into account that for better clarity the x-axis for the first (dashed line) and the second (dashed-dotted line) derivative (referring to the right y-axis) lies slightly above the x-axis for the probe current (left y-axis).

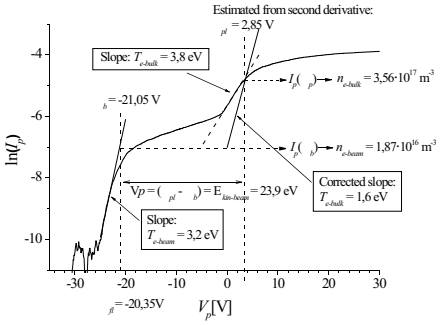

Fig. 7. Semi logarithmic plot of electron current. See the text for a detailed description of the figure.

Fig. 6 shows a typical I_p-V_p characteristic of the Langmuir probe (Fig. 5) inserted 10 mm above the muzzle of the CHC on the axis. We see a rather complicated untypical characteristic (black thick line – somewhat smoothed) with two bends, one at about V_p = –24.5 V and one at about –1.5 V. The dashed line shows the first derivative of the smoothed characteristic, the dashed-dotted line is the second derivative. If we adopt the Druyvesteyn's method, this second derivative yields the electron energy distribution (EED) [24]. However, as pointed out in [25], great care has to be taken with this method especially in plasmas where the EED is not spherically symmetric, which is obviously also not the case here.
Druyvesteyn's method has been critically and comprehensively reviewed also in [26].

Therefore we concentrate on the first derivative (dashed line) to get an idea about the possible form of the EED. This shows two maxima yielding evidence for two clearly different electron populations: a large one with the maximum at $_{pl}$ = 2.85 V and a small one with the maximum at $_b$ = –21.05 V. Obviously the large peak of the EED has to be interpreted as the bulk plasma, whereas the small peak signifies a population of electrons which has the mean kinetic energy of E_b 23.9 eV. This corresponds to the difference between the maxima of the two peaks in the EED: V_p = ($_{pl}$ – $_b$) = E_b. The latter population of the EED can be interpreted as a beam of electrons, accelerated by a DL with an approximate height of 23.9 V. Consequently, $_{pl}$ is the plasma potential determined by the bulk electrons. The beam electrons lead to additional ionization and help thus to sustain the DL. For additional corroboration of our conclusions we have logarithmized the I_p-V_p characteristic of Fig. 6, which can be seen in Fig. 7.

However, since the common method to derive the electron density and temperature utilises the electron current, first the ion current has to be defined and subtracted from the total probe current. The definition of the ion current in case of a hollow cathode is slightly difficult because of the presence of two ion species (argon ions and sputtered titanium ions). A common iteration is to define a linear fit in the ion saturation region. In this case the fit was performed in the range –90 V and –40 V and subtracted from the total probe current in the interval –90 V up to the plasma potential $_{pl}$. According to the basic probe

theory a semi-logarithmic plot of a current-voltage characteristic yields a linear relation between $\ln I_p$ and V_p in the electron retarding field region, provided the electrons possess a Maxwellian velocity distribution. Usually the electron temperature can be determined from the linear ascent of $\ln I_p(V_p)$. However, Fig. 7 shows two distinctly different parts, in which we find linear ascents of the probe electron current with the probe voltage. Hence the EED is clearly non-Maxwellian. Also this indicates the presence of two groups of electrons with different energies and densities.

Nevertheless, we can gain more information on the two electron populations from the semi-logarithmic plot, as sketched in Fig. 7. Like in the case of a purely Maxwellian velocity distribution, the slopes of the two ascents yield a measure for the electron temperatures of the two electron populations. By applying a tangent to the first linear ascent (straight solid line) between approximately –25 and –20 V, we can derive the electron temperature of beam electrons as $T_{e\text{-}beam}$ 3.2 eV, whereas the ascent of the main electron population between approximately 0 and +5 V (shown by the straight dashed line) delivers at first an uncorrected temperature of $T_{e\ bulk}^{uncorr}$ 3.8 eV. But for a precise determination of $T_{e\text{-}bulk}$, the current carried by the beam electrons has to be taken into account and a "beam-free" $\ln I_p$-V_p characteristic has to be derived, from which we can deduce the corrected value of the bulk electron temperature $T_{e\text{-}bulk}$ 1.6 eV.

By applying an analogous procedure, we can derive approximate values for the beam and bulk electron densities as $n_{e\text{-}beam}$ $1.87\ \ 10^{16}$ m^{-3} and $n_{e\text{-}bulk}$ $3.56\ \ 10^{17}$ m^{-3}, respectively. In this case we use the intersection points of the tangents (solid line and dashed line) with the vertical lines at $_b$ and $_{pl}$, respectively, as indications of the corresponding values of $\ln I_p$, from which we can deduce the electron densities. Also in this case the beam density has to be subtracted from the uncorrected value of the bulk electron density to arrive at the correct value of $n_{e\text{-}bulk}$. But due to the small value of $n_{e\text{-}beam}$ as compared to $n_{e\text{-}bulk}$, in this case the correction is very small.

3.2. Results of Ti thin film sputtering

Fig. 8a-b show examples of Ti-films for two different times of 30 and 5 s direct exposure to the plasma jet for distance d = 10 mm in front of the nozzle, for a discharge current of 20 mA and gas pressure of 0.2 mbar. The scanning area was always 500 500 nm. Finer grains are found in the sample with the shorter exposure time (Fig. 8b). Fig. 8a shows a thin white line along which a sectional scan of the height was made. This is shown in Fig. 8c. From the approximate distance between two minima (one example is indicated by the two downward arrowheads), the size of the grains was determined to be in the range between 8 and 12 nm. Hence also this result corroborates the presumption that the Ti is deposited in form of rather large clusters since the atomic radius of Ti is about 0.18 nm.

However, the above mentioned exposure times cannot be taken as the accurate deposition times of Ti-clusters, since we noticed that also in the waiting position, outside the plasma jet, Ti-films were formed on the substrate. The underlying HOPG structures (scratches and steps) are also visible in the deposited Ti films (Fig. 8a-b).

Fig. 9a shows the results of a nano-lithography carried out by means of the STM. In this case, the tunnelling current is increased from the usual value of 20 pA to 3 nA. The high current leads to evaporation of Ti-atoms and clusters from the surface so that the

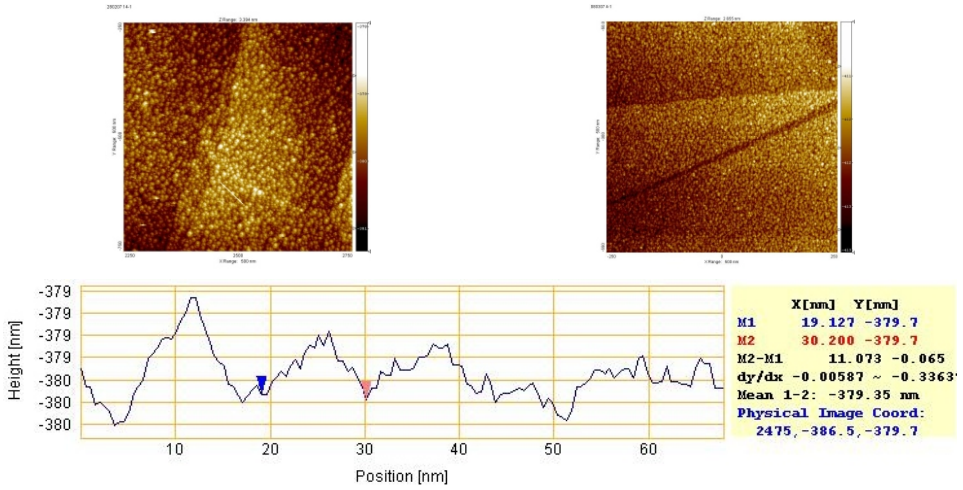

Fig. 8. Examples of thin Ti-films with area of 500 500 nm deposited on substrates of HOPG by the CHC at the Ar-pressure of 0.2 mbar, the discharge current of 20 mA and at a distance of 10 mm between the substrate and the cathode muzzle; (a) HOPG directly facing CHCSS for 30 s with scanning parameters of 2.3 V and 10 pA (b) HOPG directly facing CHCSS for 5 s with scanning parameters of 2.3 V and 20 pA (c) Sectional scan along the white line in (b).

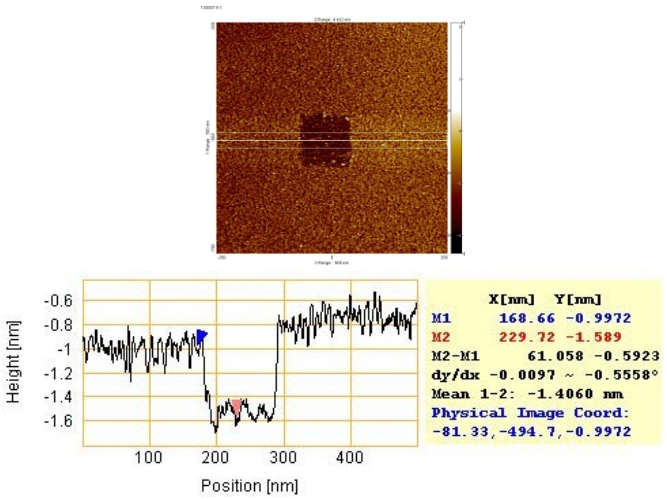

Fig. 9. (a) Example of a thin Ti-film deposited with the same parameters as in Fig. 8, with HOPG directly facing CHC for 15 s, after nano-lithography of the hole by means of the STM. Scanning parameters were 2.3 V and 20 pA, with the hole of 100 100 nm being done by setting of the tunnelling current to 2 nA for the first scan and 3 nA for the second and the third scan with the gap voltage of 2.3 V; (b) Corresponding averaged sectional scan along the white line.

graphite substrate underneath could be seen. The middle white line in Fig. 9a shows the sectional scan from which the depth of the hole could be determined as being ap-

proximately 0.6 nm (again indicated by the two downward arrowheads). This is much less than the diameter of the clusters of 8–12 nm in the horizontal plane so that we find a discrepancy between the horizontal and vertical dimensions of the clusters.

Although this discrepancy is not fully understood yet, the reasons can be that either the clusters have indeed an extremely oblate shape, or the higher state density of the HOPG that is laid open in this region, compared to the untreated titanium film, compensates most of the height change during the scan by the STM. Also the tip of the STM was not calibrated in the *z* direction.

4. Conclusion

By use of a cavity hollow cathode sputtering source (CHC), we have obtained high-quality thin films of titanium on highly oriented pyrolytic graphite (HOPG). The hollow-cathode regime of the discharge was investigated by a Langmuir probe and evidence for the formation of a plasma double layer was found in the region above the muzzle of the CHC, which produces an electron beam in addition to the bulk electrons.

The strong sputtering rate of the Ti-cathodes is provided by the hollow cathode pendulum effect of the electrons in the cavity. The sputtered Ti-atoms gather in form of clusters, which are negatively charged, in the plasma jet exiting from the CHC muzzle. The thin films were investigated by means of a scanning tunnelling microscope (STM). We have obtained from an STM scan the estimate of the cluster size as 8–12 nm. These negatively charged clusters are accelerated together with the electrons towards the grounded substrate, impinging there with a higher kinetic energy after being accelerated through the DL. In addition the pressure gradient between the internal of the hollow cathode and the space above also forces sputtered particles towards the substrate.

Thin Ti-films produced by CHC are also another possibility for nano-structuring or nano-lithography.

Acknowledgments

This work was supported by the Romanian Ministry of Education and Research, the Austrian Science Fund (through FWF-Project P14545-PHY), the CEEPUS II network AT-0063 and the Socrates-Erasmus programme.

References

[1] N. Gavrilov, G. Mesyats, G. Radkovski, V. Bersenev: Surf. Coat. Technol. **96** (1997) 81–88.
[2] K. Ishii, K. Amano, H. Hamakake: J. Vac. Sci. Technol. A **17** (1999) 310–313.
[3] E.M. Oks, A. Anders, I.G. Brown: Rev. Sci. Instrum. **75** (2004) 1030–1033.
[4] M. Pahl, F. Howorka, T. D. Märk, W. Lindinger, H. Helm: Acta Phys. Austriaca **37** (1973) 101–121.
[5] L. Bardos: Surf. Coat. Techn. 86–87 (1996) 648–656.
[6] D. Zhechev, V.I. Zhemenik, S. Tileva, G.V. Mishinsky, N. Pyrvanova: Nucl. Instr. Method. Phys. Res. B **204** (2003) 387–391.
[7] M. H. Kazemeini, A. A. Berezin, N. Fukuhara: Thin Solid Films **372** (2000) 70–77.
[8] M. H. Kazemeini. A. A. Berezin: J Vacuum Sci. Techn. A **18** (2000) 2908–2913.

[9] P. C. Balan, R. Apetrei, D. Luca, C. Ionita, R. Schrittwieser, G. Popa: J. Optoel. Adv. Mater. **7** (2005), 2459–2464.
[10] S. Guruvenket, G. Mohan Rao: J. Vac. Sci. Technol. A **20** (2002) 678–682.
[11] R. Apetrei, D. Alexandroaei, D. Luca, P. Balan, C. Ionita, R. Schrittwieser, G. Popa: Jpn. J. Appl. Phys. **45** (2006) 8128–8131.
[12] R. Apetrei, D. Alexandroaei, D. Luca, P. Balan, C. Ionita, R. Schrittwieser, G. Popa: Jpn. J. Appl. Phys. **45** (2006) 8132–8135.
[13] D. Luca: Rom. Reports in Phys. **47** (1996) 768–796.
[14] Qing Ma, R. A. Rosenberg: Phys. Rev. B **60** (1999) 2827–2832.
[15] A. D. White: J. Appl. Phys. **30** (1959) 711–719.
[16] D. J. Sturges, H. J. Oskam: Physica **37** (1967) 457–466.
[17] R. Schrittwieser, C. Ionita, D. Luca, D. Alexandroaei, R. Apetrei, V. Anita, G. Popa, P. C. Balan, S. B. Olenici, A. Murawski: 16-th Symp. Appl. Plasma Proc. –SAPP 2007 (Podbanské, Slovakia, 2007), Inv. Lect. IL10, Book of Abstracts, 75–78.
[18] R. Schrittwieser (Ed.): Proc. Fourth Symp. on Double Layers and Other Nonlinear Potential Structures in Plasmas (Innsbruck, Austria, July 6–8, 1992), World Scientific Publishing Company, Singapore, 1993, 498p.
[19] I. Langmuir: Phys. Rev. **33** (1929) 954–989.
[20] A. Murawski: Master Thesis, University of Innsbruck, Austria, 2006.
[21] A. Siebenförcher, R. Schrittwieser: Rev. Sci. Instrum. **67** (1996) 849–850.
[22] R. Schrittwieser, C. Ionita, P. C. Balan, Jose A. Cabral, H. F. C. Figueiredo, V. Pohoata, C. Varandas: Contrib. Plasma Phys. **41** (2001) 494–503.
[23] R. H. Huddelstone, S. L. Leonard: Plasma Diagnostic Techniques (Academic Press, New York London, 1965).
[24] M. J. Druyvesteyn: Z. Phys. **64** (1930) 781–798.
[25] J. A. Allen: J. Phys. D: Appl. Phys. **11** (1978) L35–L36.
[26] T. K. Popov, M. Dimitrova, F. M. Dias,V. N. Tsaneva, N. A. Stelmashenko, M. G. Blamire, Z. H. Barber: J. Phys.: Conf. Series **44** (2006) 60–69.